Journal of Materials Chemistry A

COMMUNICATION

Cite this: J. Mater. Chem. A, 2015, 3, 6271

Received 6th February 2015
Accepted 12th February 2015

DOI: 10.1039/c5ta00980d

www.rsc.org/MaterialsA

$Na_3V_2O_{2x}(PO_4)_2F_{3-2x}$: a stable and high-voltage cathode material for aqueous sodium-ion batteries with high energy density†

P. Ramesh Kumar,‡ Young Hwa Jung,‡ Chek Hai Lim and Do Kyung Kim*

The reversible electrochemical activity of the $Na_3V_2O_{2x}(PO_4)_2F_{3-2x}$ compound in an aqueous solution is reported for the first time. $Na_3V_2O_{2x}(PO_4)_2F_{3-2x}$ with multi-walled carbon nanotubes (MWCNTs) exhibits a long-term stability for up to 1100 cycles in aqueous electrolytes. Two different types of Na-ion full-cells demonstrate the feasibility of the $Na_3V_2O_{2x}(PO_4)_2F_{3-2x}$/MWCNT composite as a cathode for aqueous sodium-ion batteries. A high full-cell voltage of 1.7 V and a high energy density of 84 W h kg^{-1} were achieved using Zn metal as an anode.

As interest in alternative energy resources has increased due to concerns over global warming, much research has been focused on several rechargeable battery systems. Among the various rechargeable batteries, lithium-ion batteries (LIBs) have been employed in most of the appliances that require a portable power supply, such as electronic mobile devices. Now, LIBs are gradually expanding their areas of use into electric vehicles and energy storage systems. Simultaneously, the high cost and limited Li resources have applied pressure on fields that employ LIBs. Therefore, investigations of next-generation batteries beyond LIBs have accelerated in recent years.[1–5] As an alternative to current LIBs, sodium-ion batteries (SIBs) are potential energy storage systems that alleviate the cost and resource challenges of lithium. However, safety issues for both LIBs and SIBs based on flammable organic solvents still hinder the practical applications of SIBs. In this view, rechargeable aqueous SIBs[6,7] can overcome the shortcomings of both current LIBs and other existing aqueous batteries, such as lead acid or Ni–Cd batteries, and eliminate safety concerns and environmental toxicity.

Department of Materials Science and Engineering, Korea Advanced Institute of Science and Technology (KAIST), 291 Daehak-ro, Yuseong-gu, Daejeon 305-701, Republic of Korea. E-mail: dkkim@kaist.ac.kr

† Electronic supplementary information (ESI) available. See DOI: 10.1039/c5ta00980d

‡ These authors contributed equally to this work.

However, the narrow potential window of water and a short lifetime are the challenging points for the development of aqueous SIBs. In addition, limited electrode materials that are electrochemically active in aqueous solutions have also prevented the utilization of aqueous SIBs. Polyanion compounds have been extensively explored as alternatives to metal oxides for electrode materials in both LIBs and SIBs in recent years.[8–10] These materials exhibit structural stability with an open framework that allows for alkali ion diffusion and relatively high operating voltages due to the inductive effect of the polyanion. These characteristics may allow for the discovery of suitable electrode materials for aqueous battery systems. Recently, we reported the reversible electrochemical reaction of $Na_2FeP_2O_7$, which is a promising polyanion compound for SIBs, in a neutral aqueous solution.[11] However, $Na_2FeP_2O_7$ exhibits a low redox potential of $Fe^{2+/3+}$ despite the decent cyclability and high rate capability, resulting in aqueous SIBs with a lower energy density. Therefore, we have studied appropriate electrode materials with a focus on polyanion compounds in aqueous electrolytes to increase the overall voltage of aqueous SIBs, and herein, we report a high-voltage insertion cathode material (*i.e.*, $Na_3V_2O_{2x}(PO_4)_2F_{3-2x}$) with excellent cyclability in aqueous electrolytes. An aqueous SIB with a $Na_3V_2O_{2x}(PO_4)_2F_{3-2x}$/multi-walled carbon nanotube (MWCNT) cathode exhibits reversible Na extraction and insertion in a concentrated aqueous solution (10 M $NaClO_4$), and the highest energy density was achieved when the aqueous Na-ion full-cells were configured with Zn metal as an anode.

Fig. 1a shows the fitting results of the synchrotron X-ray diffraction (XRD) patterns of the $Na_3V_2O_{2x}(PO_4)_2F_{3-2x}$/MWCNT composite obtained from hydrothermal synthesis. The synchrotron XRD pattern was fitted using two types of tetragonal cells including $P4_2/mnm$ (no. 136) and $I4/mmm$ (no. 139). $Na_3V_2O_{2x}(PO_4)_2F_{3-2x}$ has been indexed to $P4_2/mnm$ in recent publications.[12–14] However, the observed pattern was not solely matched to only one phase. Fig. S1 (see ESI†) shows the magnified fitting results of the synchrotron XRD pattern of the $Na_3V_2O_{2x}(PO_4)_2F_{3-2x}$/MWCNT composite. The peak at 15.72°

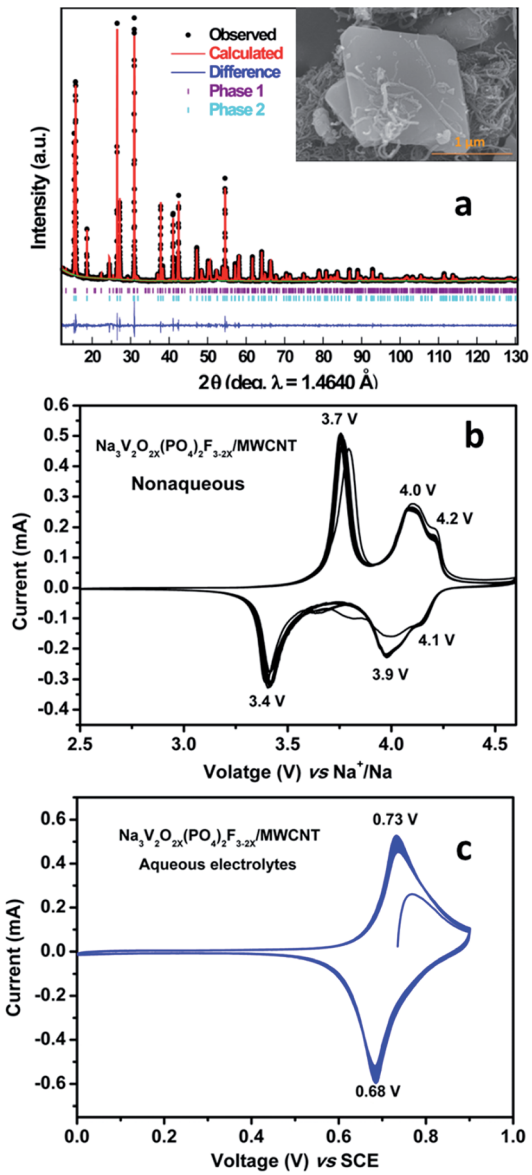

Fig. 1 (a) Synchrotron XRD data and whole pattern fitting of the $Na_3V_2O_{2x}(PO_4)_2F_{3-2x}$/MWCNT composite. Phase 1 corresponds to the $P4_2/mnm$ space group and phase 2 corresponds to the $I4/mmm$ space group. Inset shows a SEM image of the $Na_3V_2O_{2x}(PO_4)_2F_{3-2x}$/MWCNT composite. The CV results of the $Na_3V_2O_{2x}(PO_4)_2F_{3-2x}$/MWCNT composite measured at a scan rate of 0.2 mV s^{-1} in (b) non-aqueous and (c) aqueous electrolytes.

corresponds to the (0 0 2) of phase 1 ($P4_2/mnm$), and the peak at 15.78° corresponds to the (0 0 2) of phase 2 ($I4/mmm$). The fitting of phase 1 started with $Na_3V_2(PO_4)_2F_3$, as reported by Le Meins *et al.*,[15] and the initial model of phase 2 was $Na_3V_2O_2(PO_4)_2F$, as reported by Sauvage *et al.*[16] The lattice parameters in the whole pattern fitting of $Na_3V_2O_{2x}(PO_4)_2F_{3-2x}$/MWCNT ($R_p$ = 7.17%, R_{wp} = 9.58%, and χ^2 = 2.95, respectively) are refined to be a = 9.03268(8) Å, c = 10.7111(2) Å, and V = 873.914(14) Å^3 in the $P4_2/mnm$ space group (phase 1) and a = 6.38844(2) Å, c = 10.6664(3) Å, and V = 435.320(13) Å^3 in the $I4/mmm$ space group (phase 2). The as-prepared $Na_3V_2O_{2x}(PO_4)_2F_{3-2x}$ is a mixed phase of both $Na_3V_2(PO_4)_2F_3$ and $Na_3V_2O_2(PO_4)_2F$, indicating that the oxidation state of V is between +3 and +4. This oxidation state may have originated from the two-step synthesis of the composite, and the detailed synthetic process is described in the ESI.† MWCNTs are chosen to avoid the kinetic limitation of electrode materials by increasing the electronic conductivity in both aqueous and non-aqueous electrolytes. The MWCNTs are well distributed throughout the sample, as shown in Fig. S2 (ESI†). Fig. S2† shows the three different magnified SEM images and one TEM image of the $Na_3V_2O_{2x}(PO_4)_2F_{3-2x}$/MWCNT composite.

The exact oxidation state of V was further confirmed by the ^{23}Na solid-state NMR spectrum (ESI, Fig. S3†). The ^{23}Na solid-state NMR spectrum of the $Na_3V_2O_{2x}(PO_4)_2F_{3-2x}$/MWCNT composite was fitted to three main signals at 83, 106, and 152 ppm with relative intensities of 45%, 18%, and 37%, respectively. The observed chemical shifts indicate the presence of hyperfine interactions between the ^{23}Na and the paramagnetic V ions.[10,17] The three signals observed in the spectrum were assigned to the V^{4+}–V^{4+} (83 ppm), V^{3+}–V^{4+} (106 ppm), and V^{3+}–V^{3+} (152 ppm) pairs. Using the fitting data of the ^{23}NMR spectrum, we obtain an average oxidation state of the vanadium in the $Na_3V_2O_{2x}(PO_4)_2F_{3-2x}$/MWCNT composite of $V^{3.46+}$. Finally, we propose that $Na_3V_2O_{0.92}(PO_4)_2F_{2.08}$ is the general formula for the as-prepared composite material based on both the synchrotron XRD pattern and the NMR results.[12]

The inset of Fig. 1a shows the SEM image of the $Na_3V_2O_{2x}(PO_4)_2F_{3-2x}$/MWCNT composite. The as-prepared material has cube-like particles that are ~1.5 μm in size, and the MWCNTs are evenly distributed throughout the sample. The MWCNT content of the final composite was confirmed to be approximately 7.8% using the elemental analyzer. The Raman spectroscopy results for both $[V(PO_3)_3]_n$/MWCNT, which is the precursor of the final composite (see the Experimental section in the ESI†), and $Na_3V_2O_{2x}(PO_4)_2F_{3-2x}$/MWCNT composites are shown in Fig. S4 (ESI†). The Raman spectra of the two samples contain two peaks at approximately 1350 and 1580 cm^{-1}, which are attributed to the D and G bands, respectively, for the MWCNTs. In addition, the peaks at 2700 and 2910 cm^{-1} correspond to the G′ and D + G bands, respectively, for the MWCNTs. In addition to these peaks, an additional two peaks were observed in the Raman spectrum of the $Na_3V_2O_{2x}(PO_4)_2F_{3-2x}$/MWCNT composite at 930 and 1040 cm^{-1} due to the symmetric P–O stretching vibration and anti-symmetric stretching bands of the PO_4, respectively.[18,19]

To explore the electrochemical activity of $Na_3V_2O_{2x}(PO_4)_2F_{3-2x}$/MWCNTs with Na, cyclic voltammetry (CV) studies were performed at a scan rate of 0.2 mV s^{-1} in a voltage range of 4.6 V to 2.0 V *vs.* Na^+/Na. $Na_3V_2O_{2x}(PO_4)_2F_{3-2x}$/MWCNT exhibits three anodic peaks located at 3.7 V, 4.0 V and 4.2 V *vs.* Na^+/Na with corresponding cathodic peaks at 3.4 V, 3.9 V and 4.1 V *vs.* Na^+/Na, as shown in Fig. 1b. In general, there are two main redox peaks at 3.6 V and 4.1 V in $Na_3V_2O_2(PO_4)_2F$ (x = 1) with the V^{4+}/V^{5+} redox couple, while $Na_3V_2(PO_4)_2F_3$ (x = 0) exhibits a little higher potential of 3.7 V and 4.2 V with the V^{3+}/V^{4+} redox couple.[12,14,20] Since the $Na_3V_2O_{2x}(PO_4)_2F_{3-2x}$/MWCNT is the mixed phase of two compounds as discussed in Fig. 1a, the two

splitting redox peaks at the high voltage side (4.0 and 4.2 V) might be related to these compositional characteristics of our material. Fig. 1c shows the CV plot of the $Na_3V_2O_{2x}(PO_4)_2F_{3-2x}$/MWCNT composite in aqueous electrolytes in a voltage range of 0–0.9 V *vs.* SCE (0.241 V *vs.* SHE). The single anodic peak at 0.73 V and cathodic peak at 0.68 V correspond to the redox peaks at 3.7 V and 3.4 V *vs.* Na^+/Na in Fig. 1b by utilizing the single sodium ion in the structure. The potential range (0–0.9 V) was chosen to both enhance reversibility and avoid O_2 evolution at a higher voltage in aqueous electrolytes. When two sodium ions are utilized in the aqueous electrolytes, the reversibility of the $Na_3V_2O_{2x}(PO_4)_2F_{3-2x}$/MWCNT composite was poor due to electrolyte decomposition including O_2 evolution (ESI, Fig. S5†). However, the lower voltage single plateau process exhibits high reversibility over 100 cycles as confirmed in Fig. 2c. This result is in agreement with a previous result for $Na_{1.5}VOPO_4F_{0.5}$ in organic electrolytes, which was evaluated by cycling in a different voltage range.[16] In addition, a much lower polarization was observed between the anodic peak and cathodic peak in the aqueous electrolytes compared to that in non-aqueous electrolytes at the same scan rate, which is in agreement with previous results and indicates a higher ionic mobility of the aqueous solution.[11,21]

The $Na_3V_2O_{2x}(PO_4)_2F_{3-2x}$/MWCNT composite electrodes were galvanostatically charged and discharged in a voltage range of 4.5 V to 2.5 V. The cycling performance of the $Na_3V_2O_{2x}(PO_4)_2F_{3-2x}$/MWCNT composite in non-aqueous electrolytes is shown in Fig. 2a. The Na coin half-cell delivers a stable discharge capacity of 102 mA h g^{-1} with 98% coulombic efficiency at 0.1 C (13 mA g^{-1}) for 100 galvanostatic charge–discharge cycles. Fig. 2b shows the charge–discharge curves for 100 cycles of the composite. Each discharge curve shows two different plateaus of approximately the same length that are located at 3.7 and 4.1 V *vs.* Na^+/Na. The two plateaus correspond to the $V^{4+/5+}$ and $V^{3+/4+}$ redox couples as previously mentioned, and these plateaus are related to the crystal structure of the mixed valence $Na_3V_2O_{2x}(PO_4)_2F_{3-2x}$ compound. Since the main framework in the $Na_3V_2O_2(PO_4)_2F$ crystal structure is analogous to that of $Na_3V_2(PO_4)_2F_3$ except for the distortion level of the $[VO_5F]$ octahedra and substructures, the structure of the composite is assumed to be the same as that of $Na_3V_2(PO_4)_2F_3$ to understand the electrochemical behavior. Three sodium ions are located in two different sites (*i.e.*, Na1 and Na2). The first Na1 site is fully filled with two sodium ions, and the Na2 site is half filled with one sodium ion. The Na ions in the Na1 site slightly shift out of the center of the augmented prismatic sites. The Na ion in the Na2 site shifts in the opposite direction due to repulsion from the Na ion in the neighbouring Na1 site. Therefore, the extraction of the Na ion from the Na1 site requires a higher energy compared to that from the Na2 site.[20] The electrochemical performance of the $Na_3V_2O_{2x}(PO_4)_2F_{3-2x}$/MWCNT composite in aqueous electrolytes was evaluated using a beaker-type cell. A carbon paper was used as the counter electrode and a saturated calomel electrode (SCE) was used as the reference electrode in the half-cell configuration. Fig. 2c shows the cyclic stability plot for the $Na_3V_2O_{2x}(PO_4)_2F_{3-2x}$/MWCNT composite at 1 C (65 mA g^{-1}) for 100 cycles in a voltage range of 0 to 0.9 V *vs.* SCE. The half-cell delivers a stable discharge capacity of 46 mA h g^{-1} with 98% coulombic efficiency. The low capacity value is ascribed to the reversible nature of one sodium ion in an aqueous solution within the limited voltage range. The charge–discharge voltage profiles for each cycle are shown in Fig. 2d. The main attractive point of this material is its high operating potential (0.95 V *vs.* SHE) among reported Na electrode materials in aqueous electrolytes.

Fig. 3a shows the rate capability plots of the $Na_3V_2O_{2x}(PO_4)_2F_{3-2x}$/MWCNT composite cycled in non-aqueous

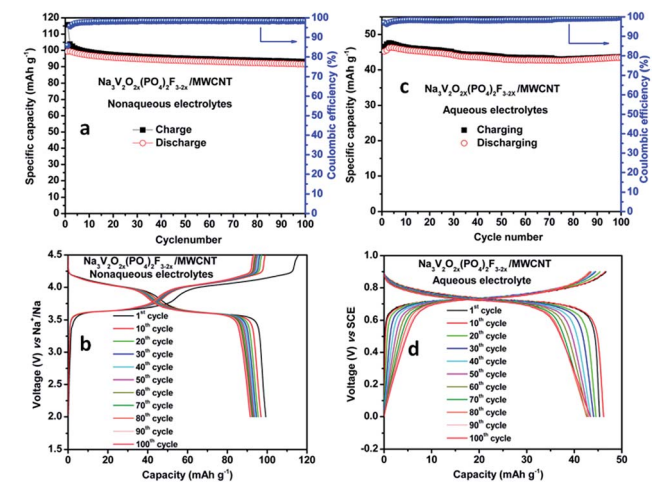

Fig. 2 (a) Cycling performance and (b) the corresponding charge–discharge voltage profiles of the $Na_3V_2O_{2x}(PO_4)_2F_{3-2x}$/MWCNT composite measured at 0.1 C (13 mA g^{-1}) in non-aqueous electrolytes. (c) Cycling performance and (d) the corresponding charge–discharge voltage profiles of the $Na_3V_2O_{2x}(PO_4)_2F_{3-2x}$/MWCNT composite measured at 1 C (65 mA g^{-1}) in aqueous electrolytes.

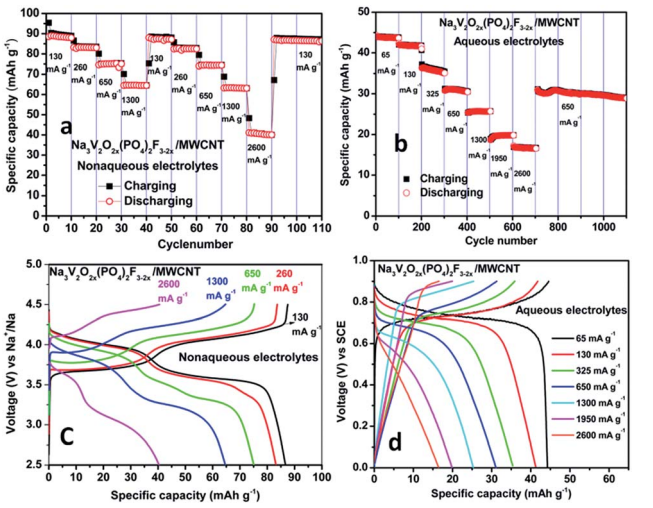

Fig. 3 (a) Rate performance and (b) representative charge–discharge voltage profiles of the $Na_3V_2O_{2x}(PO_4)_2F_{3-2x}$/MWCNT composite measured at various C-rates in non-aqueous electrolytes. (c) Rate performance and (b) representative charge–discharge voltage profiles of the $Na_3V_2O_{2x}(PO_4)_2F_{3-2x}$/MWCNT composite measured at various C-rates in aqueous electrolytes.

electrolytes at different C-rates (*i.e.*, 130 mA g^{-1} (1 C), 260 mA g^{-1} (2 C), 650 mA g^{-1} (5 C), 1300 mA g^{-1} (10 C), 2600 mA g^{-1} (20 C), and 130 mA g^{-1} (1 C)). The discharge capacity of the $Na_3V_2O_{2x}(PO_4)_2F_{3-2x}$/MWCNT composite decreases to 87, 83, 75, 65 and 41 mA h g^{-1} when the current rate was increased to 1, 2, 5, 10 and 20 C, respectively. As shown in Fig. 3b, the two plateaus corresponding to the Na ion insertion and extraction were observed even at high current rates. Fig. 3c shows the rate capability plots of the $Na_3V_2O_{2x}(PO_4)_2F_{3-2x}$/MWCNT composite cycled in aqueous electrolytes at different C-rates (*i.e.*, 65 mA g^{-1} (1 C), 130 mA g^{-1} (2 C), 325 mA g^{-1} (5 C), 650 mA g^{-1} (10 C), 1300 mA g^{-1} (20 C), 1950 mA g^{-1} (30 C), 2600 mA g^{-1} (40 C), and 650 mA g^{-1} (10 C)). The composite was tested for 100 cycles under each C-rate condition to assess the capacity retention of the composite in aqueous electrolytes. Even at a high C-rate (40 C, 2600 mA g^{-1}), the $Na_3V_2O_{2x}(PO_4)_2F_{3-2x}$/MWCNT composite retains a stable capacity of 40% of the capacity at 1 C, suggesting the high stability of the composite in aqueous electrolytes. Moreover, it is noted that an additional 400 cycles at 10 C (650 mA g^{-1}) after cycling at various C-rates were sufficient to confirm the stability of the $Na_3V_2O_{2x}(PO_4)_2F_{3-2x}$/MWCNT composite as a cathode material for aqueous SIBs. Fig. 3d shows the galvanostatic charge–discharge curves of the $Na_3V_2O_{2x}(PO_4)_2F_{3-2x}$/MWCNT composite in aqueous electrolytes with different current rates. To further confirm the structural stability of the composite after cycling, *ex situ* SEM analysis of the cycled electrode in aqueous electrolytes is performed (ESI, Fig. S6†). The morphology of the $Na_3V_2O_{2x}(PO_4)_2F_{3-2x}$/MWCNT sample is retained after 1100 cycles in aqueous electrolytes, supporting the high structural stability of the composite in an aqueous environment.

It is highly required to demonstrate the concept of a full Na-ion battery system in aqueous electrolytes for the feasibility of a new electrode material. Therefore, we have further investigated the cycling performances of the $Na_3V_2O_{2x}(PO_4)_2F_{3-2x}$/MWCNT composite as a cathode in aqueous full-cells. A Na-ion aqueous full-cell was assembled as a coin-type cell (ESI, Fig. S7a†). Fig. 4a shows the cycling performance of the Zn//$Na_3V_2O_{2x}(PO_4)_2F_{3-2x}$/MWCNT full-cell in a voltage range of 1.0 V to 2.0 V. The redox behavior of Zn metal in an aqueous solution is well known,[22,23] and recently, Zn metal was introduced as an anode for aqueous SIBs.[24] Prior to examining the electrochemical reaction for both the cathode and anode in a full-cell, a three-electrode cell was firstly tested using a flooded beaker cell (ESI, Fig. S7b†). The overpotential at the end of the first discharge voltage profile for the counter electrode (corresponding to the first charge of the working electrode) was quite high, but the polarization on the side of the counter electrode gradually decreased by further cycling. The deposition process on the Zn metal in the initial few cycles may not be facile due to a lack of Zn ions to plate and the passivation layer of the bare Zn metal. Therefore, we assigned a pre-cycling step with a wide voltage range (1–2.3 V) before the actual cycling tests for the Zn//$Na_3V_2O_{2x}(PO_4)_2F_{3-2x}$/MWCNT coin full-cell to facilitate the redox reaction of the anode. The initial capacity at 1 C (65 mA g^{-1}) for the Zn//$Na_3V_2O_{2x}(PO_4)_2F_{3-2x}$/MWCNT full-cell was 54 mA h g^{-1} based on the mass of the cathode, and 85% (46 mA h g^{-1}) of the initial

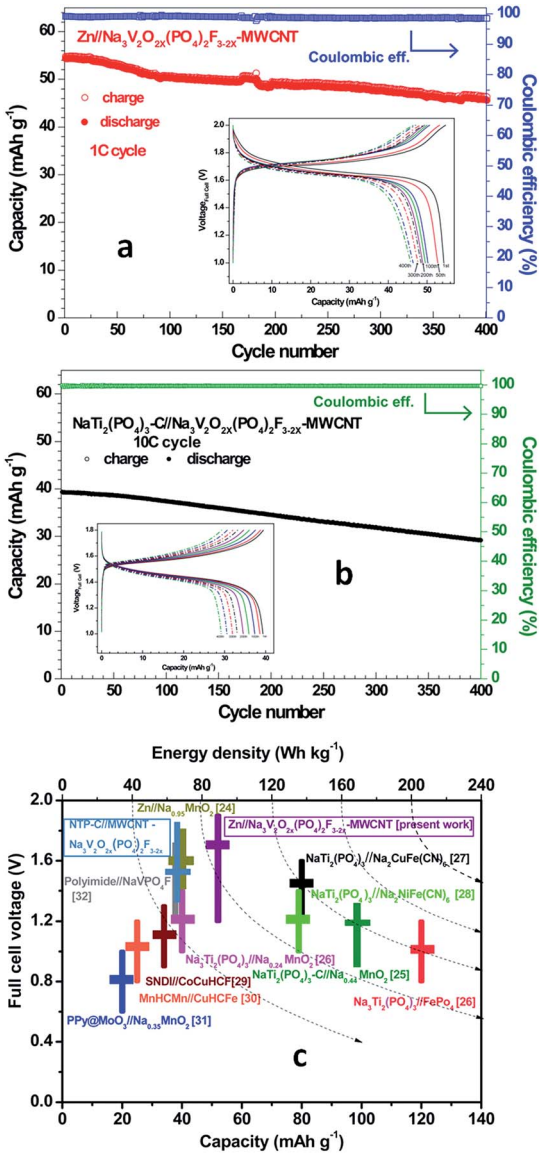

Fig. 4 Cycling performance and coulombic efficiencies of the (a) Zn//$Na_3V_2O_{2x}(PO_4)_2F_{3-2x}$/MWCNT full-cell and (b) $NaTi_2(PO_4)_3$–C//$Na_3V_2O_{2x}(PO_4)_2F_{3-2x}$/MWCNT full-cell in aqueous electrolytes. Inset shows the corresponding charge–discharge voltage profiles of the given full-cell. (c) Comparison of the capacity, energy density and full-cell voltage reported for aqueous sodium-ion batteries. The capacity is calculated on the basis of the cathode material.

capacity was retained after 400 cycles. The average coulombic efficiency was 98.9 (±0.25)%, suggesting a high reversibility for the Na-ion full-cell despite the over-voltage range of the aqueous solution. The discharging voltage for this full-cell was 1.65 V resulting in an energy density of 84 W h kg^{-1} based on both the cathode and anode, which is one of the highest values for aqueous SIBs.

Furthermore, we have demonstrated another Na-ion aqueous full-cell using $NaTi_2(PO_4)_3$–C as an anode. The XRD pattern, morphology, CV, and galvanostatic cycling results of the $NaTi_2(PO_4)_3$–C half-cell in aqueous electrolytes are shown in Fig. S8 (ESI†). The $NaTi_2(PO_4)_3$–C//$Na_3V_2O_{2x}(PO_4)_2F_{3-2x}$/MWCNT full-cell

also exhibited a stable cycling performance at a high rate of 10 C (650 mA g^{-1}) in a range between 1.0 and 1.8 V as shown in Fig. 4b. A discharge capacity of 30 mA h g^{-1} (75% of the initial capacity) was achieved after 400 cycles with an excellent average coulombic efficiency of 99.6 (±0.07)%. As the operating potential for $NaTi_2(PO_4)_3$ was ~0.2 V higher than that for Zn, the discharge voltage for the $NaTi_2(PO_4)_3$–C//$Na_3V_2O_{2x}(PO_4)_2F_{3-2x}$/MWCNT full-cell was 1.45 V. The capacity, voltage, and energy density for the aqueous Na-ion full-cells are compared in Fig. 4c. The capacity and energy density are calculated based only on the mass of the cathode. Various aqueous SIBs, such as $NaTi_2(PO_4)_3$//$Na_{0.44}MnO_2$,[25] $Na_3Ti_2(PO_4)_3$//$Na_{0.24}MnO_2$,[26] $NaTi_2(PO_4)_3$//Na_2-$CuFe(CN)_6$,[27] $NaTi_2(PO_4)_3$//$Na_2NiFe(CN)_6$,[28] $Na_3Ti_2(PO_4)_3$//$FePO_4$,[26] disodium naphthalene diimide (SNDI)//cobalt and copper hexacyanoferrate (CoCuHCF),[29] manganese hexacyanomanganate (MnHCMn)//copper hexacyanoferrate (CuHCFe),[30] Zn//$Na_{0.95}MnO_2$,[24] PPy@MoO_3//$Na_{0.35}MnO_2$,[31] and polyimide//$NaVPO_4F$[32] have been previously studied. Our results are consistent with the results from these studies, and the Zn//$Na_3V_2O_{2x}$-$(PO_4)_2F_{3-2x}$/MWCNT full-cell in this study exhibits the highest voltage with a comparable energy density exceeding 80 W h kg^{-1}.

Conclusions

The $Na_3V_2O_{2x}(PO_4)_2F_{3-2x}$/MWCNT composite enables a reversible sodium ion extraction/insertion into its structure with a high rate capability and excellent cyclability in both non-aqueous and aqueous electrolytes. In particular, the reversible electrochemical reaction of the $Na_3V_2O_{2x}(PO_4)_2F_{3-2x}$ compound in an aqueous solution is reported for the first time. In addition, two different types of coin full-cells were assembled to confirm the feasibility of the $Na_3V_2O_{2x}(PO_4)_2F_{3-2x}$/MWCNT composite as a cathode in aqueous SIBs. A high full-cell voltage of 1.7 V and a high energy density of 84 W h kg^{-1} were achieved by using Zn metal as the anode. Decent cyclic stabilities of the two aqueous Na-ion full-cells were also confirmed using the $Na_3V_2O_{2x}$-$(PO_4)_2F_{3-2x}$/MWCNT composite as a cathode. These characteristics indicate that the mixed valence polyanion compound is a promising candidate as a cathode material for both Na-ion non-aqueous and inexpensive aqueous batteries.

Acknowledgements

Authors gratefully acknowledge financial support from the Program to Solve Climate Changes (NRF-2010-C1AAA001-2010-0029031) of Korea (NRF) funded by the Ministry of Science, ICT & Future Planning.

Notes and references

1 J. M. Tarascon, *Philos. Trans. R. Soc., A*, 2010, **368**, 3227.
2 J. B. Goodenough and K. S. Park, *J. Am. Chem. Soc.*, 2013, **135**, 1167.
3 S. Y. Hong, Y. Kim, Y. Park, A. Choi, N. S. Choi and K. T. Lee, *Energy Environ. Sci.*, 2013, **6**, 2067.
4 M. D. Slater, D. Kim, E. Lee and C. S. Johnson, *Adv. Funct. Mater.*, 2013, **23**, 947.
5 V. Palomares, M. C. Cabanas, E. C. Martinez, M. H. Han and T. Rojo, *Energy Environ. Sci.*, 2013, **6**, 2312.
6 Z. Chang, Y. Yang, M. Li, X. Wang and Y. Wu, *J. Mater. Chem. A*, 2014, **2**, 10739.
7 H. Kim, J. Hong, K. Y. Park, H. Kim, S. W. Kim and K. Kang, *Chem. Rev.*, 2014, **114**, 11788.
8 C. Masquelier and L. Croguennec, *Chem. Rev.*, 2013, **113**, 6552.
9 M. S. Whittingham, *Chem. Rev.*, 2004, **104**, 4271.
10 C. G. Grey and N. Dupre, *Chem. Rev.*, 2004, **104**, 4493.
11 Y. H. Jung, C. H. Lim, J. H. Kim and D. K. Kim, *RSC Adv.*, 2014, **4**, 9799.
12 P. Serras, V. Palomares, J. Alonso, N. Sharma, J. M. López del Amo, P. Kubiak, M. Luisa Fdez-Gubieda and T. Rojo, *Chem. Mater.*, 2013, **25**, 4917.
13 P. Serras, V. Palomares, T. Rojo, H. E. A. Brand and N. Sharma, *J. Mater. Chem. A*, 2014, **2**, 7766.
14 Y. U. Park, D. H. Seo, H. Kim, J. Kim, S. Lee, B. Kim and K. Kang, *Adv. Funct. Mater.*, 2014, **24**, 4603.
15 J. M. Le Meins, M. P. Crosnier-Lopez, A. Hemon-Ribaud and G. Courbion, *J. Solid State Chem.*, 1999, **148**, 260.
16 F. Sauvage, E. Quarez, J. M. Tarascon and E. Baudrin, *Solid State Sci.*, 2006, **8**, 1215.
17 B. L. Ellis, T. N. Ramesh, L. J. M. Davis, G. R. Goward and L. F. Nazar, *Chem. Mater.*, 2011, **23**, 5138.
18 R. Vidano and D. B. Fischbach, *J. Am. Ceram. Soc.*, 1978, **61**, 13.
19 H. Nii, Y. Sumiyama, H. Nakagawa and A. Kunishige, *Appl. Phys. Express*, 2008, **1**, 064005.
20 R. A. Shakoor, D. H. Seo, H. Kim, Y. U. Park, J. Kim, S. W. Kim, H. Gwon, S. Lee and K. Kang, *J. Mater. Chem.*, 2012, **22**, 20535.
21 D. J. Kim, R. Ponraj, A. G. Kannan, H. W. Lee, R. Fathi, R. Ruffo, C. M. Mari and D. K. Kim, *J. Power Sources*, 2013, **244**, 758.
22 L. Zhang, L. Chen, X. Zhou and Z. Liu, *Adv. Energy Mater.*, 2015, **5**, 1400930.
23 J. Yan, J. Wang, H. Liu, Z. Bakenov, D. Gosselink and P. Chen, *J. Power Sources*, 2012, **216**, 222.
24 B. Zhang, Y. Liu, X. Wu, Y. Yang, Z. Chang, Z. Wen and Y. Wu, *Chem. Commun.*, 2014, **50**, 1209.
25 Z. Li, D. Young, K. Xiang, W. C. Carter and Y. M. Chiang, *Adv. Energy Mater.*, 2013, **3**, 290.
26 Z. Li, D. B. Ravnsbæk, K. Xiang and Y. M. Chiang, *Electrochem. Commun.*, 2014, **44**, 12.
27 X. Y. Wu, M. Y. Sun, Y. F. Shen, J. F. Qian, Y. L. Cao, X. P. Ai and H. X. Yang, *ChemSusChem*, 2014, **7**, 407.
28 X. Wu, Y. Cao, X. Ai, J. F. Qian and H. Yang, *Electrochem. Commun.*, 2013, **31**, 145.
29 D. J. Kim, Y. H. Jung, K. K. Bharathi, S. H. Je, D. K. Kim, A. Coskun and J. W. Choi, *Adv. Energy Mater.*, 2014, **4**, 1400133.
30 M. Pasta, C. D. Wessells, N. Liu, J. Nelson, M. T. McDowell, R. A. Huggins, M. F. Toney and Y. Cui, *Nat. Commun.*, 2014, **5**, 3007.
31 Y. Liu, B. H. Zhanga, S. Y. Xiao, L. L. Liu, Z. B. Wen and Y. P. Wu, *Electrochim. Acta*, 2014, **116**, 512.
32 H. Qin, Z. P. Song, H. Zhan and Y. H. Zhou, *J. Power Sources*, 2014, **249**, 367.